Direct evidence of Mg diffusion through threading mixed dislocations in GaN p–n diodes and its effect on reverse leakage current ᴇᴘ

View Online   Export Citation   CrossMark

Shigeyoshi Usami,[1,a)] Norihito Mayama,[2] Kazuya Toda,[2] Atsushi Tanaka,[3,4] Manato Deki,[3] Shugo Nitta,[3] iD
Yoshio Honda,[3] and Hiroshi Amano[3,4,5,6]

AFFILIATIONS

[1] Graduate School of Engineering, Nagoya University, Nagoya 464-8603, Japan
[2] Toshiba Nanoanalysis Corporation, Yokohama 235-8522, Japan
[3] Institute of Materials and Systems for Sustainability, Nagoya University, Nagoya 464-8601, Japan
[4] National Institute of Material Science, Ibaraki 305-0047, Japan
[5] Akasaki Research Center, Nagoya University, Nagoya 464-8603, Japan
[6] Venture Business Laboratory, Nagoya University, Nagoya 464-8603, Japan

a) Electronic mail: s_usami@nuee.nagoya-u.ac.jp

ABSTRACT

Mg diffusion is a common problem in GaN devices with p–n junctions. Although this impurity diffusion is reported to occur through threading dislocations (TDs), no direct evidence has yet been obtained. Therefore, we tried the direct observation of Mg diffusion by atom probe tomography (APT) analysis. The n-type drift layer of the fabricated p–n diode was exposed, and etch pits were formed on the drift layer to identify the TD position. The APT analysis around TDs was carried out by lifting out the drift layer around specific etch pits using a focused ion beam to include TDs. The relationship between the etch pit shape and the TD type was confirmed by cross-sectional scanning transmission electron microscopy observation. The APT analysis of two types of etch pits formed on the mixed dislocations was performed, and Mg diffusion was clearly observed through the mixed dislocations. In this work, we show direct evidence of Mg diffusion via mixed dislocations in GaN p–n diodes and its effect on reverse leakage current.

Published under license by AIP Publishing. https://doi.org/10.1063/1.5097767

GaN is a direct-transition semiconductor that can be modulated in a wide range of bandgap energies from 0.7 to 6.2 eV by alloying with InN or AlN and thus has been used for light-emitting device applications such as light-emitting diodes (LEDs) and laser diodes (LDs). In recent years, it has been considered a promising power semiconductor material owing to its high critical breakdown electric field, high electron mobility, and high electron saturation velocity. A p–n junction is an important component in these devices, and precise interface control is essential for improving the device characteristics. Mg is used as an acceptor of GaN; however, owing to its high activation energy ($\sim 245 \pm 25$ meV),[1,2] high-concentration doping at 10^{19} cm^{-3} or higher is required to obtain a high hole concentration. Mg doped at a high concentration diffuses to the underlying n-type layer or active layer by heat during the growth of the p-type layer or the aging of LDs.[3] In the case of GaN on a sapphire substrate, which has a high threading dislocation density (TDD), considerable Mg

diffusion occurs. It is reported that Mg diffuses through threading dislocations (TDs).[3,4] However, direct evidence of Mg diffusion through TDs has not yet been obtained, and it is still unclear whether Mg indeed diffuses along the TDs. Therefore, we tried to analyze impurity diffusion into TDs by atom probe tomography (APT). APT is an analysis method that combines field-emission microscopy and time-of-flight mass spectrometry and can be used to observe constituent atoms of a specimen three-dimensionally. With the development of pulsed-laser-assisted APT, it is applied to not only metals but also semiconductors. For example, alloy composition analysis[5] or impurity segregation analysis[6] can be performed. This method has a high spatial resolution of subnanometer scale and a relatively low detection limit of an atomic concentration of approximately 5×10^{18} cm^{-3}; thus, it can be applied to the analysis of impurity diffusion into TDs. In this paper, we report on the analysis of Mg diffusion by APT for specific TDs in p–n diodes and its effect on reverse leakage current.

The evaluation procedure used in this study is shown in Fig. 1. A vertical p–n diode having an n-type drift layer was fabricated, and a schematic cross section of the p–n diode is shown in Fig. 1(a). Specifically, a 200 nm n^+-GaN layer (Si, 3×10^{18} cm^{-3}), a 13 μm n-GaN drift layer (Si, 2×10^{16} cm^{-3}), a 600 nm p-GaN layer (Mg, 4×10^{19} cm^{-3}), and a 30 nm p^+-GaN contact layer (Mg, $>1 \times 10^{20}$ cm^{-3}) were grown by metal-organic vapor phase epitaxy (MOVPE) on a free-standing n-GaN substrate with a TDD of 3×10^6 cm^{-2}. The TDD was measured by the wafer providers. The p–n diode structure was grown at 750 hPa, and the growth temperature of all the layers was 1030 °C. The use of a free-standing substrate with a low TDD allows us to evaluate TDs individually.

The p–n diodes were fabricated as follows. First, deep etching of about 10 μm was performed by inductively coupled plasma-reactive ion etching (ICP-RIE) using pure Cl$_2$ gas to isolate each device and mitigate the electric field crowding at the device edge.[7] Then, a p-type layer was activated at 700 °C for 5 min by rapid thermal annealing (RTA) in a nitrogen atmosphere. The Ni/Au ohmic contact to the p-type layer was deposited using an electron beam evaporator and sintered by RTA at 525 °C for 5 min in an oxygen atmosphere. Polyimide was applied as a coating to prevent the discharge of electricity in air

when a high reverse voltage was applied. Finally, Al was deposited as a back-side ohmic contact by sputtering. The bottom electrode had a window immediately under the mesa for emission observation. This p–n diode was the same as the MP-PND (a p-n diode grown under 750 hPa) in Ref. 8. The circular mesa diameter of the measured diodes was 540 μm. The corresponding electrode diameter was 500 μm.

The forward and reverse I–V characteristics of the p–n diodes were measured using a semiconductor parameter analyzer (Keysight, B1505A) and are shown in Fig. 2. To reduce the influence of the impurity diffusion due to current heating, the current compliances were set to 1 and 8 mA in reverse and forward I–V measurements, respectively. All the reverse I–V curves showed nondestructive breakdown at −900 V and a relatively high leakage current. From the forward I–V curve, it is found that the minimum ideality factor was 1.6 at 2.8 V. This value was slightly higher than that of another group's p–n diodes.[9] This increase is probably due to damage of the mesa surface caused by etching. The variation of the forward current was not related to the amount of reverse leakage current and may have been due to the fluctuation of the contact resistance of the p electrode.

The leakage position was observed by emission microscopy (Hamamatsu Photonics, PHEMOS-1000), and a representative emission image is shown in Fig. 3(a). The density of the observed leakage spots was 1.5×10^3 cm^{-2}. This was about 1/2000 of the total TDD in the device. After I–V and leakage spot characterization, the polyimide and the electrode were dissolved. Then, the p-type layer was etched by ICP-RIE to expose the drift layer near the p–n junction. By this method, we investigated only the Mg that diffused in the drift layer. Etch pits were formed by dipping the exposed drift layer in molten KOH to identify the TD position. Figure 3(b) shows an optical microscopy (OM) image after KOH etching at 450 °C for 1 min. When we observed the KOH etched drift-layer by scanning electron microscopy (SEM), four types of etch pits were identified, referred to as large, medium, small, and very small in the descending order of diameter. Figures 3(c)–3(f) show SEM images of each type of etch pit. Note here that very small pits were not counted in Ref. 8. When we overlaid the positions of the leakage spots on the OM image after KOH etching, the leakage spots coincided with some of the large pits and no medium
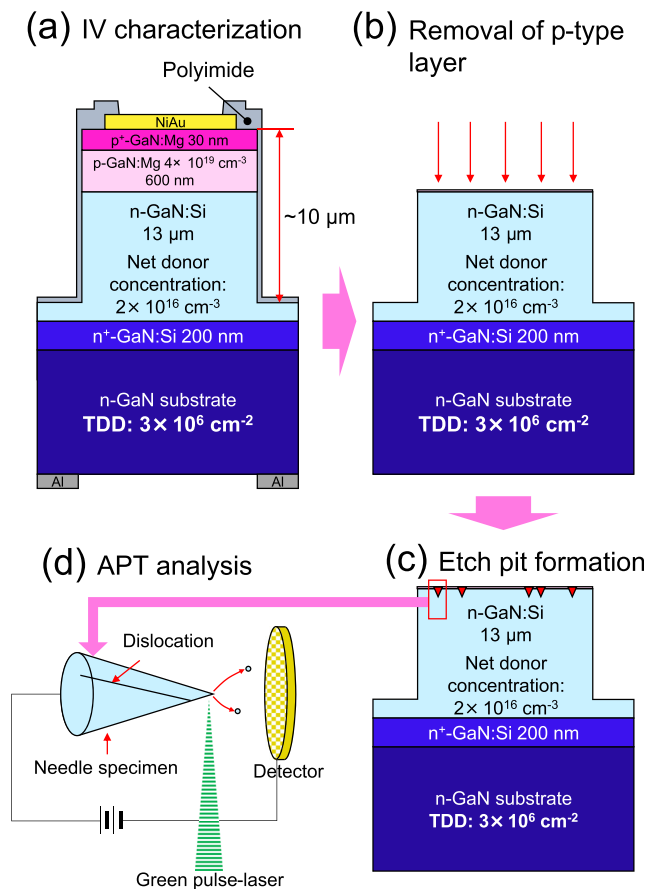

FIG. 1. Evaluation procedure. (a) Schematic cross section of the fabricated p–n diode. (b) Removal of the polyimide, electrode, and p-type layer. (c) Etch pit formation using molten KOH. (d) APT analysis under a specific etch pit.
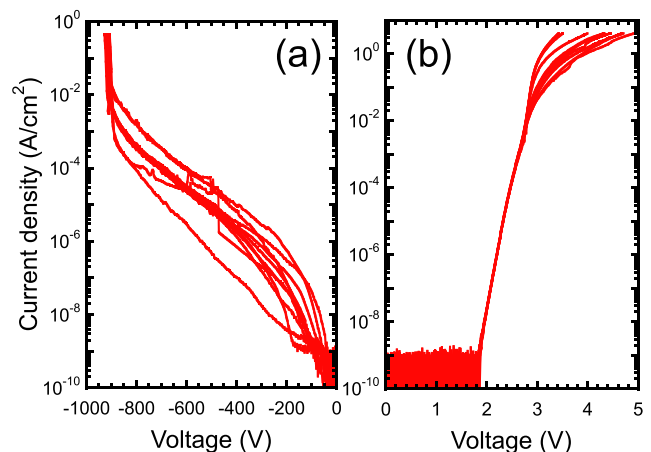

FIG. 2. I–V characteristics under (a) reverse and (b) forward bias conditions. The electrode diameter is 500 μm.
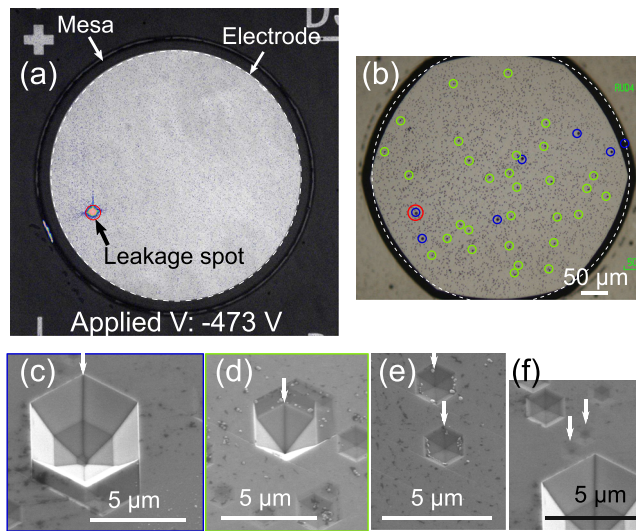
FIG. 3. (a) Emission image of the p–n diode. (b) OM image after the p-type layer removal and KOH etching. SEM images of (c) large, (d) medium, (e) small, and (f) very small pits. The remaining p-GaN was observed as a bright contrast inside the etch pit. Red, blue, and light green circles denote the positions of the leakage spot, large pit, and medium pit, respectively.

FIG. 4. Cross-sectional STEM images of medium, small, and very small pits under $g = [11\bar{2}0]$ and $g = [0002]$ conditions. The medium and small pits were formed on mixed dislocations. The very small pit was formed on edge dislocations. Segments m and e indicate the mixed and edge dislocations, respectively.

pits coincided with the leakage spots, as shown in Fig. 3(b). Very rarely, small/very small pits and leakage spots appeared to coincide, but almost all the small/very small pits did not coincide with the leakage spots. Since the etch pit shape reflects the TD type,[10–17] the TD types of all etch pit types were identified on the basis of the invisibility criterion for $g \cdot b = 0$, where g is the reciprocal lattice vector and b is the Burgers vector of the TD, by cross-sectional scanning transmission electron microscopy (STEM) observation. The observed GaN thin films under the etch pits were prepared by the standard focused ion beam (FIB)-assisted lift-out process.

We have already reported that a large pit was formed on nanopipes in Ref. 8. The low leakage spot density compared to the total TDD is due to the low nanopipe density in this p–n diode. Figure 4 shows STEM images of medium, small, and very small pits. Under the medium and small pits, contrast of the dislocation line was observed under both $g = [11\bar{2}0]$ and $g = [0002]$ conditions. Therefore, it was determined that the medium and small pits were formed on the mixed dislocations. These findings indicate that there were two types of mixed dislocations in our p–n diodes. On the other hand, in the case of a very small pit, the dislocation line almost disappeared under the $g = [0002]$ condition. A TD that shows such behavior is an edge dislocation.

In this study, we selected the medium and small pits for APT analysis. Since a nanopipe has a hollow core, we can induce sample destruction by high-electric-field application in APT; and therefore, it was excluded as an observation target. In addition, very small pits were not observed because the pit diameter was extremely small and visual recognition by FIB/SEM was difficult.

As shown in Fig. 4, since the wall surface angle of the pits differs with the TD type, the depth of the medium pit was $\sim4\,\mu m$, whereas that of the small pit was $\sim400\,nm$ in the case of 450 °C KOH etching. To make the distances from the p–n interface as equal as possible, a
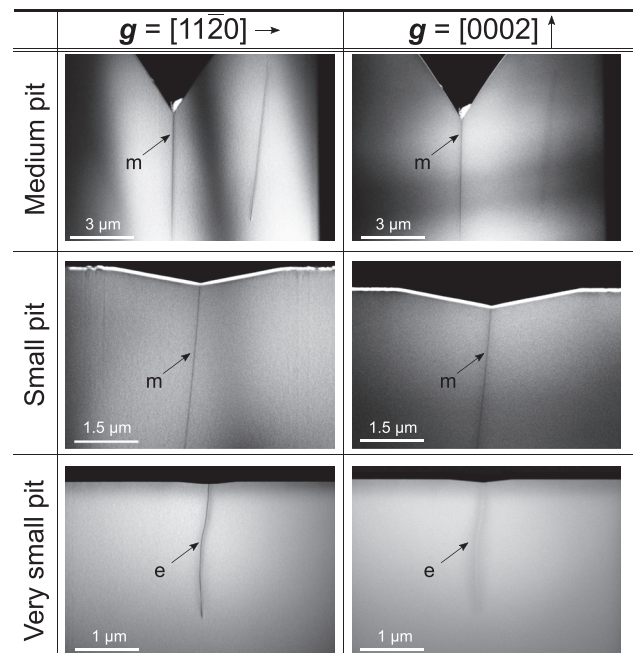
medium pit was newly formed by KOH etching at 350 °C for 1 min. Under this condition, the depth of the medium pit became about 300 nm. Medium and small pits of similar etch depths were analyzed by APT. Neither type of pit coincided with the leakage spots under high reverse bias conditions.

The selected etch pit was lifted out from the exposed drift layer using FIB. Then, it was also annularly milled by FIB centered on the etch pit to prepare a needle-shaped specimen (needle specimen) containing a TD under the etch pit. The final milling process was performed at a low acceleration voltage of 2 kV so that the effect of Ga-ion implantation into the TDs was minimized. For the APT analysis, we used a LEAP 3000XSi in the laser-pulse mode. The laser had a wavelength of 532 nm and was applied at a pulse repetition rate of 0.5 MHz. The pulse energy was about 0.01 nJ. The flight length between the specimen and the detector was approximately 90 mm. The analyses were performed at 30 K at a detection rate of 0.002 at./pulse. The needle specimen containing a TD was set for the APT analysis and subjected to a large forward voltage. When the pulsed laser is irradiated on a specimen, the surface atoms may ionize, and ions leave from the specimen's apex. Then, the ions are accelerated to the detector that is sensitive to the impact position of the ions and to their time-of-flight. The time-of-flight of the ions allows the determination of their mass/charge ratio. The obtained mass spectra thus allow the determination of the chemical composition of the specimen. The data of the detected ion position and mass/charge ratio collected after each laser pulse were combined to form a three-dimensional tomographic image of the specimen through a back-projection algorithm. In this way, the impurity diffusing into TDs was analyzed.

STEM images of the fabricated needle specimen with medium and small pits are shown in Fig. 5(a). The STEM images show that both needle specimens contain a TD. Note here that the top of the needle specimen is not just below the pit because we were unable to capture the center of the pit during the sample milling. Therefore, the precise distance from the p–n interface to the tip of the needle specimens is unknown. From the depth of the etch pits, the medium and small pits were separated by at least 300 and 400 nm from the p–n interface, respectively. Using these needle specimens, we carried out APT analysis. The measured tomographic images of Mg under medium and small pits are shown in Fig. 5(b). The lengths of the needle specimens measured by APT were approximately 300 and 200 nm under the medium and small pits, respectively. The Mg tomographic images clearly show the Mg distribution along both mixed dislocations. Although it appears that Mg is distributed throughout the needle specimens, this widespread distribution is due to noise. From the measured mass spectra, Mg was not detected in any region except the dislocation region. The observed diameter of the region with distributed Mg was about 4 nm. Since the spatial resolution might be degraded around TDs, the accuracy of the measurement of the spread of Mg around TDs may be low. It is necessary to analyze by simulation (e.g., density functional theory) whether diffused Mg exists in the core of TDs or around TDs.

From the APT data, isoconcentration surfaces with 0.4 at. % Mg were generated and are shown in Fig. 5(c). The isoconcentration surface under the medium pit shows the decreasing concentration of Mg along TDs with the increasing distance from the p–n interface. This indicates that Mg from p-GaN diffused through the mixed dislocations. On the other hand, Mg appears to be uniformly distributed and showed no diffusion profile along the mixed dislocations under the small pit. This may be due to the fact that the actual distance from the p–n interface to the tip of the needle specimen was much smaller for the small pits than for the medium pits. Alternatively, it may be due to the incorporation of residual Mg into the mixed dislocations during the growth of the drift layer. To distinguish these two possibilities, it is necessary to evaluate the dependence on the Mg concentration or the growth temperature of p-GaN by APT.

By adding the pit depth and length measured by APT, we determined that Mg diffused or became incorporated to a depth of at least 500 nm at a concentration of $>10^{19}$ cm^{-3} for the mixed dislocations that form medium and small pits. Furthermore, no leakage spots were observed at these mixed dislocations. Therefore, it is revealed that the Mg diffusion or incorporation into the mixed dislocations does not generate leakage current.

In summary, we investigated Mg diffusion through TDs in p–n diodes. Among the etch pits (large, medium, small, and very small) formed on the exposed drift layer, the medium and small pits were examined by APT analysis of the TDs under them. Medium and small pits were identified as mixed dislocations by cross-sectional STEM observation. As a result of the analysis, the Mg diffusion was confirmed in mixed dislocations under medium pits. This result provides direct evidence of Mg diffusion into mixed dislocations. For the small pits, further investigation is required as to determine whether Mg diffuses or is incorporated into TDs. From the correlation with leakage spots, it was revealed that this Mg diffusion or incorporation through the mixed dislocations did not cause the leakage current. Since this method has been shown to be effective for the observation of impurity diffusion into TDs, analysis of screw and edge dislocations is under way.

FIG. 5. (a) STEM images of needle specimens with medium and small pits. (b) XZ plane projection views of three-dimensional tomographic images of Mg. (c) Isoconcentration surface with 0.4 at. % Mg. Owing to the setup of the APT analysis, the center of the needle specimen tends to be affected by noise. Mg was not detected except in the dislocation region.

REFERENCES

[1]S. Brochen, J. Brault, S. Chenot, A. Dussaigne, M. Leroux, and B. Damilano, Appl. Phys. Lett. **103**, 032102 (2013).
[2]M. Horita, S. Takashima, R. Tanaka, H. Matsuyama, K. Ueno, M. Edo, T. Takahashi, M. Shimizu, and J. Suda, Jpn. J. Appl. Phys. Part 1 **56**, 031001 (2017).
[3]S. N. Lee, H. S. Paek, J. K. Son, H. Kim, K. K. Kim, K. H. Ha, O. H. Nam, and Y. Park, J. Electroceram. **23**, 406 (2009).
[4]N. Kuroda, C. Sasaoka, A. Kimura, A. Usui, and Y. Mochizuki, J. Cryst. Growth **189/190**, 551 (1998).
[5]B. Bonef, M. Lopez-Haro, L. Amichi, M. Beeler, A. Grenier, E. Robin, P. H. Jouneau, N. Mollard, I. Mouton, B. Haas, E. Monroy, and C. Bougerol, Nanoscale Res. Lett. **11**, 461 (2016).
[6]S. Khromov, D. Gregorius, R. Schiller, J. Lösch, W. Wahl, M. Kopnarski, H. Amano, B. Monemar, L. Hultman, and G. Pozina, Nanotechnology **25**, 275701 (2014).
[7]H. Fukushima, S. Usami, Y. Ando, A. Tanaka, M. Deki, M. Kushimoto, S. Nitta, Y. Honda, and H. Amano, Appl. Phys. Express **12**, 026502 (2019).
[8]S. Usami, A. Tanaka, H. Fukushima, Y. Ando, M. Deki, S. Nitta, Y. Honda, and H. Amano, Jpn. J. Appl. Phys. Part 1 **58**, SCCB24 (2019).
[9]K. Nomoto, B. Song, Z. Hu, M. Zhu, M. Qi, N. Kaneda, T. Mishima, T. Nakamura, D. Jena, and H. G. Xing, IEEE Electron Device Lett. **37**, 161 (2016).
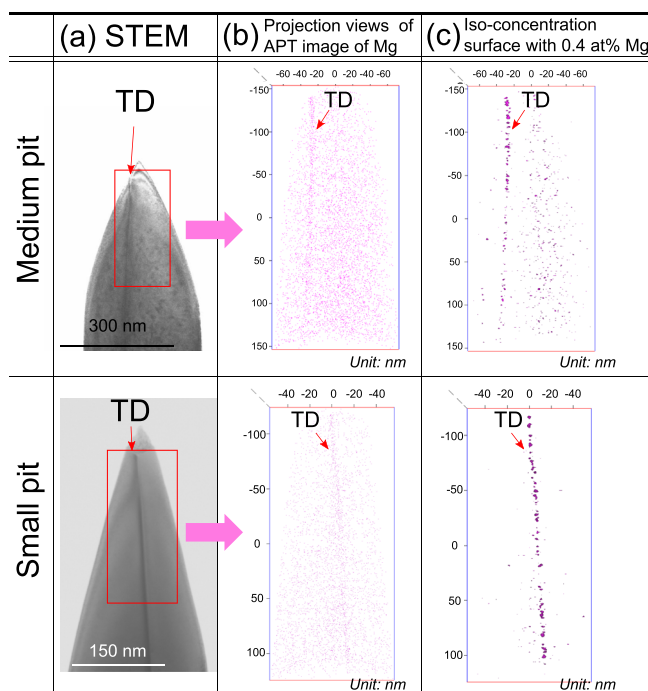
[10]S. K. Hong, B. J. Kim, H. S. Park, Y. Park, S. Y. Yoon, and T. I. Kim, J. Cryst. Growth **191**, 275 (1998).

[11]T. Hino, S. Tomiya, T. Miyajima, K. Yanashima, S. Hashimoto, and M. Ikeda, Appl. Phys. Lett. **76**, 3421 (2000).

[12]J. L. Weyher, Superlattices Microstruct. **40**, 279 (2006).

[13]J. Chen, J. F. Wang, H. Wang, J. J. Zhu, S. M. Zhang, D. G. Zhao, D. S. Jiang, H. Yang, U. Jahn, and K. H. Ploog, Semicond. Sci. Technol. **21**, 1229 (2006).

[14]J. L. Weyher, S. Lazar, L. Macht, Z. Liliental-Weber, R. J. Molnar, S. Müller, V. G. M. Sivel, G. Nowak, and I. Grzegory, J. Cryst. Growth **305**, 384 (2007).

[15]L. Lu, Z. Y. Gao, B. Shen, F. J. Xu, S. Huang, Z. L. Miao, Y. Hao, Z. J. Yang, G. Y. Zhang, X. P. Zhang, J. Zu, and D. P. Yu, J. Appl. Phys. **104**, 123525 (2008).

[16]L. Zhang, Y. Shao, W. X. Hao, X. Chen, S. Qu, and X. Xu, J. Alloys Compd. **504**, 186 (2010).

[17]Y. Yao, Y. Ishikawa, Y. Sugawara, D. Yokoe, M. Sudo, N. Okada, and K. Tadatomo, Superlattices Microstruct. **99**, 83 (2016).